CHAPTER 8 Boundary conditions and nested grids

8.1 Introduction

Boundary conditions can be real or fictitious. At a real wall, the normal component of the velocity vanishes, which implies that no mass crosses the wall.

The Earth's surface is a "real wall" at the lower boundary of the atmosphere. Many models also have "ficititious walls" at their tops.

With some vertical coordinate systems (such as height), topography imposes a lateral boundary condition in an atmospheric model. Ocean models describe flows in basins, and so (depending again on the vertical coordinate system used) have "real" lateral boundary conditions.

Limited area models have artificial lateral boundaries. Even global models are limited-domain models in the sense that they have physical lower boundaries and artificial "lids."

Models in which the grid spacing changes rapidly (e.g. nested grid models) effectively apply boundary conditions where the dissimilar grids meet.

This chapter deals with the effects of boundary conditions, with emphasis on what can go wrong.

8.2 Inflow Boundaries

Consider advection in an artificially bounded domain. Instead of prescribing initial values of the advected quantity u for all x, *we prescribe u at* $x = 0$ *for all time*. In particular, we assume $u(t)$ at $x = 0$ as a simple harmonic function, with frequency ω. Note that we can choose ω as we please. Referring again to the advection equation, i.e.

$$\frac{\partial u}{\partial t} + c\frac{\partial u}{\partial x} = 0 , \tag{8.1}$$

we assume $c > 0$ and write

$$u(x, t) = Re[U(x)e^{-i\omega t}], \qquad \omega \neq 0 . \tag{8.2}$$

We prescribe $U(0)$ as a real constant. Then

$$u(0, t) = U(0)Re(e^{-i\omega t}) = U(0)\cos\omega t . \tag{8.3}$$

Since $c > 0$, we have effectively prescribed an "inflow" or "upstream" boundary condition.

Use of (8.3) in (8.1) gives

$$-i\omega U + c\frac{dU}{dx} = 0 , \tag{8.4}$$

which has the solution

$$U(x) = U(0)e^{ikx} . \tag{8.5}$$

The dispersion equation is obtained by substituting (8.5) into (8.4):

$$\omega = ck . \tag{8.6}$$

The full solution is thus

$$\begin{aligned} u(x, t) &= U_0 Re\{exp[i(kx - \omega t)]\} \\ &= U_0 Re\{exp[ik(x - ct)]\} . \end{aligned} \tag{8.7}$$

Now consider the same problem again, this time as represented through the differential-difference equation

$$\frac{du_j}{dt} + c\left(\frac{u_{j+1} - u_{j-1}}{2\Delta x}\right) = 0 . \tag{8.8}$$

We assume a solution of the form

$$u_j = Re[U_j e^{-i\omega t}] , \tag{8.9}$$

we obtain the now-familiar dispersion relation

$$\omega = ck\frac{\sin(k\Delta x)}{k\Delta x} . \tag{8.10}$$

This should be compared with (8.6). Fig. 8.1 gives a schematic plot, with $\omega\Delta x/c$ and $k\Delta x$ as coordinates, for the true dispersion equation (8.6) and the approximate dispersion equation (8.10). The results are plotted only out to $k\Delta x = \pi$, which corresponds to $L = 2\Delta x$, the shortest resolvable wave. *For a given* ω we have one k in the exact solution. In the numerical solution, however, we have two k's, which we are going to call k_1 and k_2. As discussed below,

for $\omega > 0$, k_1 corresponds to the exact solution. Note that

$$k_2 \Delta x = \pi - k_1 \Delta x . \tag{8.11}$$

Also note that the group velocity is positive for $k\Delta x < \pi/2$, and negative for $k\Delta x > \pi/2$.

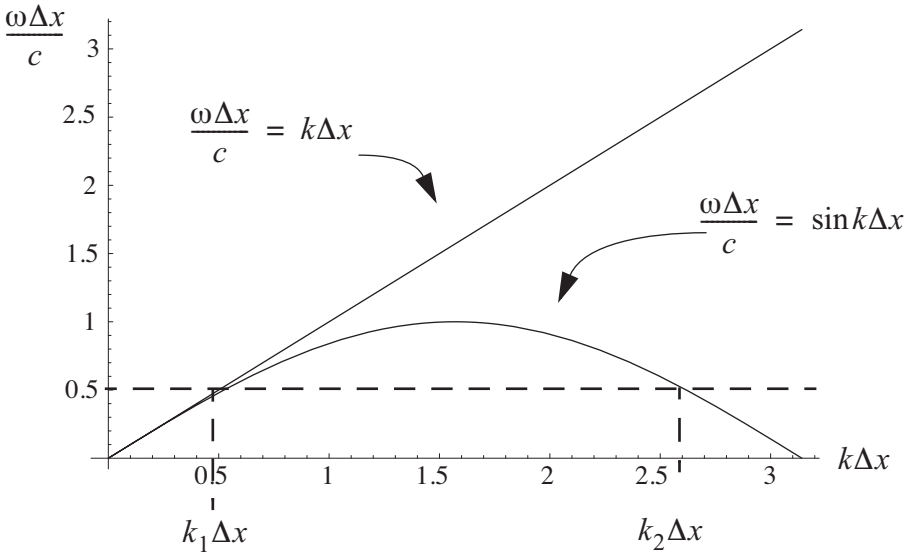

Figure 8.1: A schematic plot, with $\frac{\omega \Delta x}{c}$ and $k\Delta x$ as coordinates, for the true solution (8.3) and the approximate solution (8.10). The dashed line illustrates that for a given ω the approximate solution allows two different wave numbers.

When we studied the leapfrog time-differencing scheme in Chapter 3, we had a somewhat similar result. In Chapter 3 we had two solutions with different frequencies for a given wavelength. Here we have a single given frequency but two solutions of differing wavelength associated with that frequency. We can call the solution corresponding to k_1 a "physical mode" in space, and the solution corresponding to k_2 a "computational" mode in space. Notice that the wavelength that corresponds to k_2, i.e. the wavelength of the computational mode, will always be between $2\Delta x$ (which corresponds to $k\Delta x = \pi$) and $4\Delta x$ (which corresponds to $k\Delta x = \frac{\pi}{2}$). For $k_1 \Delta x > \frac{\pi}{2}$, there really is no physical mode. In other words, *the physical mode exists only for* $L \geq 4\Delta x$. In view of (8.12), $k_1 \Delta x < \frac{\pi}{2}$, which is the requirement that a physical mode exists, corresponds to $sin^{-1}\left(\frac{\omega \Delta x}{c}\right) < \frac{\pi}{2}$. This condition can be satisfied by choosing Δx small enough, for given values of ω and c.

Referring back to (8.10), we see that the two modes can be written as

$$\text{physical mode:} \quad u_j \sim Re\left\{\exp\left[ik_1\left(j\Delta x - \frac{\omega}{k_1}t\right)\right]\right\}, \tag{8.12}$$

$$\begin{aligned}\text{computational mode:} \quad u_j &\sim Re\left\{\exp\left[ik_2\left(j\Delta x - \frac{\omega}{k_2}t\right)\right]\right\} \\ &= Re\{\exp[i(j\pi - k_1 j\Delta x - \omega t)]\} \\ &= (-1)^j Re\left\{\exp\left[-ik_1\left(j\Delta x + \frac{\omega}{k_1}t\right)\right]\right\},\end{aligned} \tag{8.13}$$

where $k_2\Delta x = \pi - k_1\Delta x$ and $e^{ij\pi} = (-1)^j$ have been used, note that the two modes will have different amplitudes. The phase velocity of the computational mode is opposite to that of the physical mode, and it oscillates in space with wave length $2\Delta x$, due to the factor of $(-1)^j$.

In general, the solution is a superposition of the physical and computational modes. In case $c > 0$ and the point $j = 0$ is the "source of influence," like a smoke stack, only a physical mode appears for $j > 0$ and only a computational mode appears for $j < 0$. Fig. 8.2 shows this schematically for some arbitrary time. The dashed line for $j < 0$ represents (8.13),

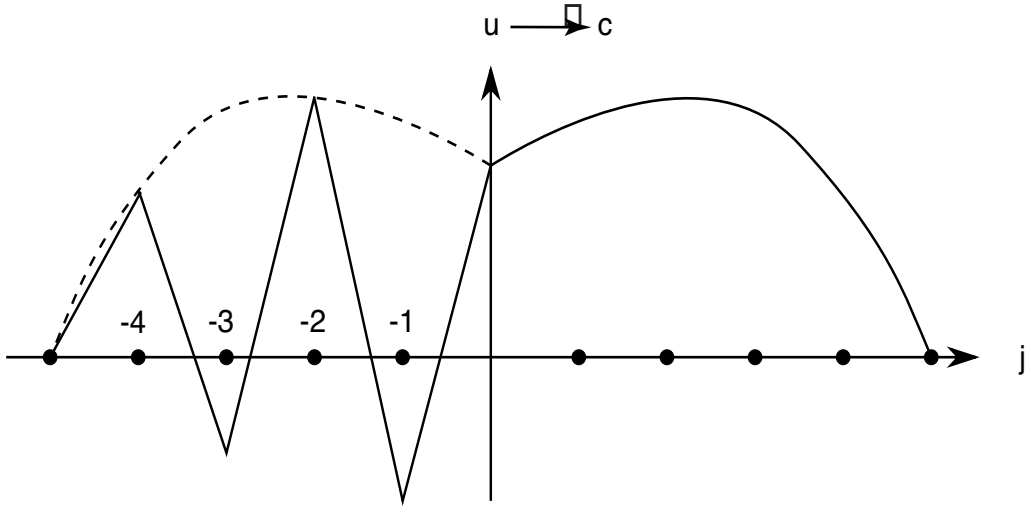

Figure 8.2: Schematic illustration of a computational mode that is restricted to the domain $j < 0$, and a physical mode that is restricted to the domain $j > 0$.

without the factor $(-1)^j$; the solid line represents the entire expression. The influence of the computational mode propagates to the left. If the wave length of the physical mode is very large (compared to Δx), the computational mode will appear as an oscillation from point to point, i.e. a wave of length $2\Delta x$.

According to (8.10), the apparent phase change per grid interval, Ω, is related to the wave number by

$$\Omega \equiv \frac{\omega \Delta x}{c} = \sin(k\Delta x) \cong k\Delta x \text{ for } k\Delta x \ll 1 . \tag{8.14}$$

With the exact equations, $\Omega = k\Delta x$. Since we control ω, Δx, and c, we effectively control Ω. Suppose that we give $\Omega > 1$, by choosing a large value of Δx. In that case, in order to satisfy (8.14), k must be complex:

$$k = k_r + ik_i . \tag{8.15}$$

To see what this means, we write

$$\begin{aligned}
\sin(k\Delta x) &= -\frac{i}{2}(e^{ik\Delta x} - e^{-ik\Delta x}) \\
&= -\frac{i}{2}[e^{ik_r\Delta x - k_i\Delta x} - e^{-ik_r\Delta x + k_i\Delta x}] \\
&= -\frac{i}{2}e^{-k_i\Delta x}[\cos(k_r\Delta x) + i\sin(k_r\Delta x)] - e^{k_i\Delta x}[\cos(k_r\Delta x) - i\sin(k_r\Delta x)] \\
&= \frac{1}{2}\{[e^{-k_i\Delta x}\sin(k_r\Delta x) + e^{k_i\Delta x}\sin(k_r\Delta x)] + i[-e^{-k_i\Delta x}\cos(k_r\Delta x) + e^{k_i\Delta x}\cos(k_r\Delta x)]\} \\
&= \sin(k_r\Delta x)\cosh(k_i\Delta x) + i\cos(k_r\Delta x)\sinh(k_i\Delta x) .
\end{aligned} \tag{8.16}$$

Substituting back into (8.14), and equating real and imaginary parts, we conclude that

$$\begin{aligned}
\Omega &= \sin(k_r\Delta x)\cosh(k_i\Delta x), \\
0 &= \cos(k_r\Delta x)\sinh(k_i\Delta x).
\end{aligned} \tag{8.17}$$

We cannot have $\sinh(k_i\Delta x) = 0$, because this would imply $k_i\Delta x = 0$. Hence

$$\cos(k_r\Delta x) = 0, \text{ which implies that } k_r\Delta x = \frac{\pi}{2}. \tag{8.18}$$

This is the 4 - Δx wave, for which

$$\sin(k_r\Delta x) = 1 , \tag{8.19}$$

and so from (8.17) we find that

$$k_i \Delta x = \cosh^{-1}(\Omega) > 0 . \tag{8.20}$$

The inequality follows because $\Omega > 1$ by hypothesis. We can now write (8.9) as

$$u_j = U_0 e^{-i\omega t} e^{ik_r j\Delta x} e^{-k_i j\Delta x} . \tag{8.21}$$

Since $k_i > 0$, u_j damps as $j \to \infty$.

Suppose that we use an uncentered scheme in place of (8.8), e.g.

$$\frac{\partial u_j}{\partial t} + \frac{c}{\Delta x}(u_j - u_{j-1}) = 0 , \tag{8.22}$$

with $c > 0$. we will show that the uncentered scheme damps regardless of the values of w, Δx, and c. Let

$$u_j = U e^{-i\omega t} e^{ikj\Delta x} , \tag{8.23}$$

$$u_{j-1} = U e^{-i\omega t} e^{ik(j-1)\Delta x} . \tag{8.24}$$

Then we obtain

$$-i\omega + \frac{c}{\Delta x}(1 - e^{-ik\Delta x}) = 0. \tag{8.25}$$

First, suppose that k is real. Setting the real and imaginary parts of (8.25) to zero gives

$$\begin{aligned} \cos k\Delta x &= 1 , \\ -\omega + ck\left[\frac{\sin(k\Delta x)}{k\Delta x}\right] &= 0 . \end{aligned} \tag{8.26}$$

Since $\cos k\Delta x = 1$ implies that $k\Delta x = 0$, this solution is not acceptable. We conclude that k must be complex.

Accordingly, use (8.15) to obtain

$$k = k_r + ik_i . \tag{8.27}$$

Then we obtain

$$-i\omega + \frac{c}{\Delta x}(1 - e^{-ik_r\Delta x}e^{k_i\Delta x}) = 0 . \tag{8.28}$$

Setting the real part to zero gives:

$$1 - e^{k_i\Delta x}\cos(k_r\Delta x) = 0 . \tag{8.29}$$

Setting the imaginary part to zero gives:

$$\Omega + e^{k_i\Delta x}\sin(k_r\Delta x) = 0 . \tag{8.30}$$

These two equations can be solved for the two unknowns k_r and k_i. Let

$$\begin{aligned} X &\equiv e^{k_i\Delta x} , \\ Y &\equiv k_r\Delta x , \end{aligned} \tag{8.31}$$

Then

$$\begin{aligned} 1 - X\cos(Y) &= 0 , \\ -\Omega = X\sin(Y) &= 0 , \end{aligned} \tag{8.32}$$

which implies that

$$\begin{aligned} X &= \sec Y , \\ \tan Y &= \Omega , \end{aligned} \tag{8.33}$$

from which it follows that

$$X = \sec[\tan^{-1}(\Omega)] > 1 . \tag{8.34}$$

From (8.34) and (8.31), we see that $k_i > 0$. Substituting back, we obtain

$$u_j = Ue^{-i\omega t}e^{ik_r j\Delta x}e^{-k_i j\Delta x} . \tag{8.35}$$

This shows that, as $j \to \infty$, the signal weakens.

Exercise: Repeat the analysis above, starting from $\frac{u_j^{n+1} - u_j^{n-1}}{2\Delta t} + c\left(\frac{u_{j+1} - u_{j-1}}{2\Delta x}\right) = 0 .$

8.3 Outflow boundaries

So far we have assumed that the initial condition is given everywhere on the space axis, but now we consider a case in which it is given only in a certain limited domain. To illustrate, in Fig. 8.3, lines of constant $x - ct$ are shown. If the initial condition is specified at

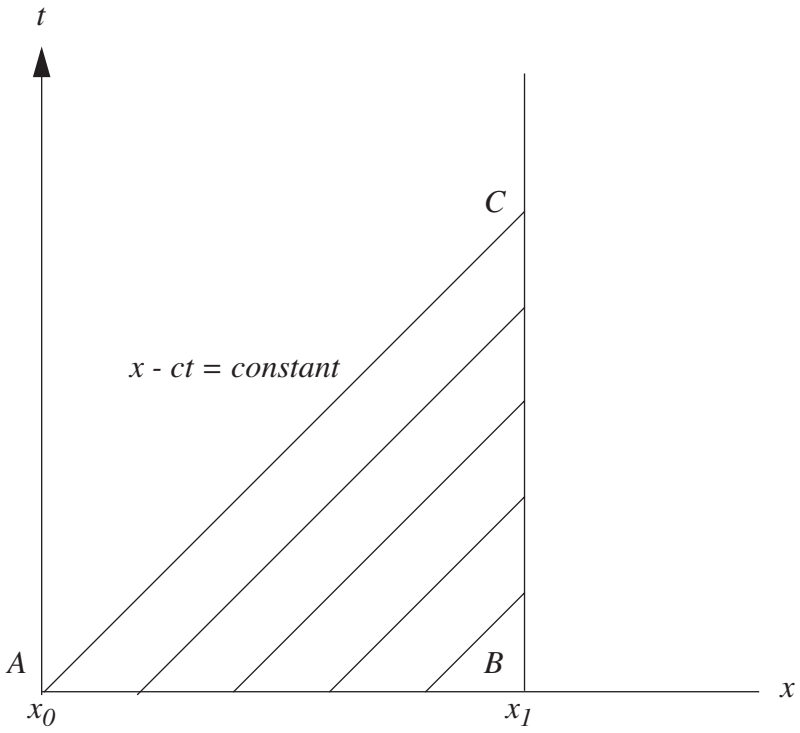

Figure 8.3: An initial condition that is specified between $x = x_0$ and $x = x_1$ determines the solution only along the characteristics shown.

$t = 0$, between the points A ($x = x_0$, $t = 0$), and B ($x = x_1$, $t = 0$), then $u(x, t)$ is determined in the triangular domain ABC. To determine $u(x, t)$ above the line AC, we need a boundary condition for $t > 0$ at $x = x_0$. When this boundary condition and the initial condition at $t = 0$ between the points A and B are specified, we can obtain the solution within the entire domain $(x_0 \le x \le x_1)$. If the subsidiary conditions are given so that the solution exists and is determined uniquely, we have a well-posed problem. Note that a boundary condition at $x = x_1$ is of no use.

Suppose that we are carrying out our numerical solution of (8.1) over the region between $j = 0$ and $j = J$, as shown in Fig. 8.4, using leapfrog time-differencing and centered space-differencing, i.e.

$$\frac{u_j^{n+1} - u_j^{n-1}}{2\Delta t} + c\left(\frac{u_{j+1} - u_{j-1}}{2\Delta x}\right) = 0 , \tag{8.36}$$

and that we are given u at $j = 0$ as a function of time. At $j = 1$ we can write, using centered space differencing,

$$\frac{\partial u_1}{\partial t} + c\left(\frac{u_2 - u_0}{2\Delta x}\right) = 0 , \tag{8.37}$$

At $j = J - 1$ we have

$$\frac{\partial u_{J-1}}{\partial t} + c\left(\frac{u_J - u_{J-2}}{2\Delta x}\right) = 0 . \tag{8.38}$$

Eq. (8.38) shows that in order to predict u_{J-1}, we need to know u_J. We need to give a condition on u_J as a function of time, or in other words, a "*computational boundary condition*." Unless we are integrating over the entire globe or are dealing with some other specific problem in which spatial periodicity of the solution can be assumed, we must specify an artificial boundary condition at the point J; see Fig. 8.4. Ideally, this artificial boundary condition should not affect the interior in any way, since its only purpose is to limit (for computational purposes) the size of the domain.

Figure 8.4: An outflow boundary condition must be specified at *j = J*, in this finite and non-periodic domain.

For the case of the continuous advection equation, we can give boundary conditions only at the inflow point, but for the finite-difference equation we also need a computational boundary condition at the outflow point.

With the leapfrog scheme, we needed two initial conditions. The current situation is somewhat analogous. Essentially, both problems arise because of the three-level differences (one in time, the other in space) used in the respective schemes. If the computational boundary condition is not given properly, there is a possibility of exciting a strong computational mode.

Nitta (1964) presented some results of integrating the advection equation with leapfrog time differencing, using various methods of specifying the computational boundary condition. Nitta's paper deals mainly with space differencing, but as discussed later his conclusions are influenced by his choice of leapfrog time differencing. Table 8.1 summarizes the boundary conditions or "Methods" that Nitta considered. The results that he obtained are

shown in Fig. 8.5.

Table 8.1: A summary of the computational boundary conditions studied by Nitta.

Method 1	$u_J = \text{constant in time}$
Method 2	$u_J^n = u_{J-1}^n$
Method 3	$\left(\frac{du}{\partial t}\right)_J = \left(\frac{du}{\partial t}\right)_{J-1}$
Method 4	$u_J^n = u_{J-2}^n$
Method 5	$u_J^n = 2u_{J-1}^n - u_{J-2}^n$
Method 6	$\left(\frac{du}{\partial t}\right)_J = 2\left(\frac{du}{\partial t}\right)_{J-1} - \left(\frac{du}{\partial t}\right)_{J-2}$
Method 7	$\left(\frac{du}{dt}\right)_J = -c\left(\frac{u_J^n - u_{J-1}^n}{\Delta x}\right)$
Method 8	$\left(\frac{du}{dt}\right)_J = -\frac{c}{2\Delta x}(3u_J - 4u_{J-1} + u_{J-2})$

With Method 1, u_J is constant in time. With Method 2, $u_J^{(n)} = u_{J-1}^{(n)}$, i.e. the first derivative of u vanishes at the wall. With Method 4, $u_J^{(n)} = u_{J-2}^{(n)}$, which is similar to Method 2. Method 5, on the other hand, sets $u_J^{(n)} = 2u_{J-1}^{(n)} - u_{J-2}^{(n)}$, a linear extrapolation of the two interior points to $u_J^{(n)}$. This is equivalent to setting the second derivative to zero at the wall. Method 7 predicts u_J by means of

$$\frac{u_J^{(n+1)} - u_J^{(n-1)}}{2\Delta t} + \frac{u_J^{(n)} - u_{J-1}^n}{\Delta x} = 0 , \tag{8.39}$$

which uses uncentered differencing in space. This is equivalent to using $u_{J+1} = 2u_{J-1}$, which is very similar to Method 5. For this reason, Methods 5 and 7 give very similar results. Method 8 is similar to Method 7, but has higher-order accuracy.

Recall that, with respect to the spatial dimension, the "physical" mode is given by $u_j \propto \exp\left[ik_1\left(j\Delta x - \frac{\omega}{k_1}t\right)\right]$ and the "computational" mode is given by $u_j \propto (-1)^j \exp\left[-ik_1\left(j\Delta x + \frac{\omega}{k_1}\right)t\right]$. Since the computational mode propagates "upstream," we wish to examine the solution at the outflow boundary in order to determine the "initial" amplitude of the computational mode excited there. We assume that the domain extends far upstream towards decreasing j. In general, our solution can be expressed as a linear combination of the two modes. Referring to (8.12) and (8.13), we can write

$$u_j = U_0 Re\left\{\exp\left[ik\left(j\Delta x - \frac{\omega}{k}t\right)\right] + r(-1)^j \exp\left[-ik\left(j\Delta x + \frac{\omega}{k}t\right)\right]\right\}, \tag{8.40}$$

where k is the wave number of the physical mode and r is the virtual reflection rate at the boundary for the computational mode, so that $|r|$ is the ratio of the amplitude of the computational mode to that of the physical mode. We would like to make $r = 0$.

We now do an analysis to try to understand why Nitta obtained these results.

In Method 1, u_J is kept constant. Assume $u_J = 0$, for simplicity, and let J be even ("without loss of generality"). We then can write from (8.40)

$$u_J = U_0\{\exp[ikJ\Delta x] + r\exp[-ikJ\Delta x]\}\exp[-i\omega t] = 0, \tag{8.41}$$

or, since $e^{-i\omega t} \neq 0$, we conclude that

$$r = \frac{-\exp[ikJ\Delta x]}{\exp[-ikJ\Delta x]} = -\exp[2ikJ\Delta x], \tag{8.42}$$

which implies that $|r| = 1$. *This means that the incident wave is totally reflected*. The computational mode's amplitude is equal to that of the physical mode - a very unsatisfactory situation, as can be seen from Fig. 8.5.

With Method 2, and still assuming that J is even, we put $u_J = u_{J-1}$. Then we obtain

$$\exp[ikJ\Delta x] + r\exp[-ikJ\Delta x] = \exp[ik(J-1)\Delta x] - r\exp[-ik(J-1)\Delta x], \tag{8.43}$$

which reduces to $|r| = \tan\frac{k\Delta x}{2}$. For $L = 4\Delta x$, we get $|r| = 1$. Recall that $L < 4\Delta x$ need not be considered. For large L, we get $|r| \to 0$, i.e. very long waves are not falsely reflected. In Fig. 8.5, the incident mode is relatively long.

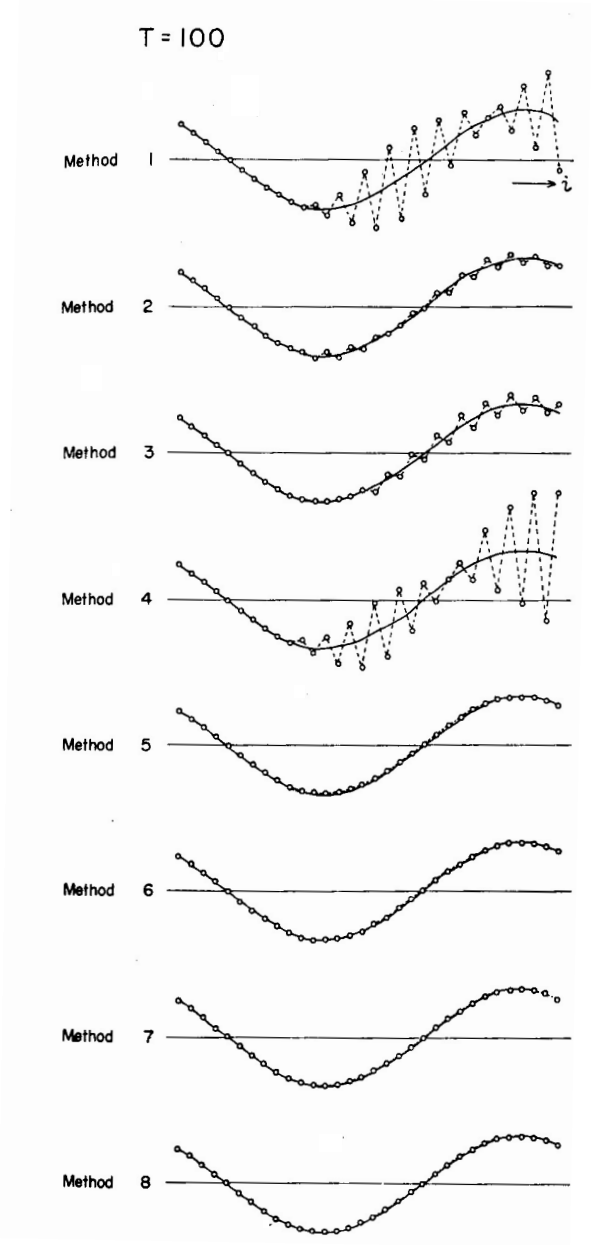

Figure 8.5: A summary of Nitta's numerical results, with various computational boundary conditions. Here leapfrog time differencing was used.

With Method 5, it turns out that $|r| = \tan^2\left(\frac{k\Delta x}{2}\right)$. Fig. 8.6 is a graph of $|r|$ versus $k\Delta x$ for Methods 1, 2, and 5. Because k is the wave number of the physical mode, we only

consider $k\Delta x$ between 0 and $\frac{\pi}{2}$; it is only in this region that we have a "physical" mode corresponding to the real solution. Higher-order extrapolations give even better results for the lower wave numbers, but there is little motivation for doing this.

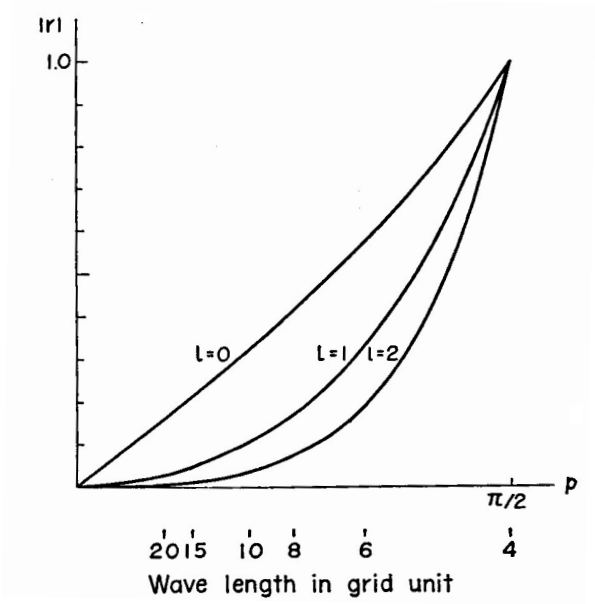

Figure 8.6: A graph of $|r|$ versus $k\Delta x$ for Methods 1, 2, and 5. From Matsuno (1966).

In actual computations one must also have an inflow boundary, and *this will then act as an outflow boundary for the computational mode which has propagated back upstream*. A secondary mode will then be reflected from the inflow boundary and will propagate downstream, and so on. There exists the possibility of multiple reflections back and forth between the boundaries. Can this process amplify in time, as in a laser? Platzman's (1954) conclusion, *for the leapfrog scheme*, was that specification of u_j constant on the outflow boundary - and not an extrapolation from nearby points - is necessary for stability.

Therefore, we have a rather paradoxical situation, at least with the leapfrog scheme. If we use Method 1, the domain is quickly filled with small scale "noise," but this "noise" remains stable. If we use Methods 5 or 7, the domain will only be littered with "noise" after a considerable length of time (depending on the width of the domain and the velocity c), but once the noise becomes noticeable, it will continue to grow and the model will blow up.

This situation is analogous to using the leapfrog scheme with a friction term specified at the central time level. There is an energy loss in the solution domain through the boundaries when using Method 5 or 7. In Method 1, all of the energy is held, whereas in Methods 5 and 7 some of it is lost due to incomplete reflection at the outflow boundary.

A more complete model with a larger domain would in fact permit energy to pass out through the artificial boundaries of the smaller domain considered here. The schemes that permit such loss, namely 5 and 7, are therefore more realistic, but nevertheless they can cause an instability. This could be avoided by use of a different time differencing scheme.

8.4 Advection on nested grids

If we use an inhomogeneous grid (one in which the grid size varies), we will encounter a problem similar to the one met at the boundaries; a reflection occurs because the fine portion of the grid permits short waves that cannot be represented on the coarse portion of the grid. This is a serious difficulty with all models that use nested grids. The problem can be minimized by various techniques, but it cannot be eliminated.

Consider the one-dimensional advection equation

$$\frac{\partial u}{\partial t} + c\frac{\partial u}{\partial x} = 0\,,\ c > 0\,. \tag{8.44}$$

We wish to solve this equation on a grid in which the grid size changes suddenly at $j = 0$, from d_1 to d_2, as shown below:

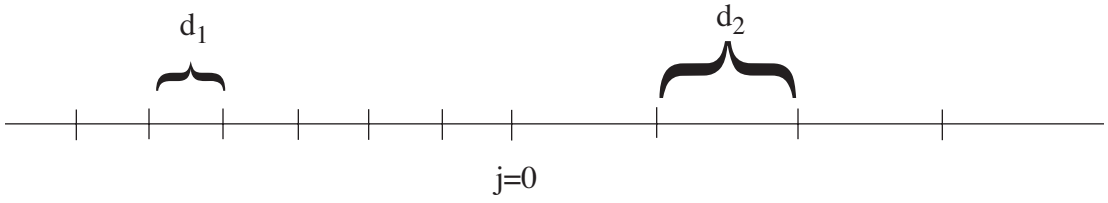

The sketch shows $d_2 > d_1$, but we will also consider the opposite case. We use the following differential-difference equations:

$$\frac{du_j}{dt} + c\left(\frac{u_{j+1} - u_{j-1}}{2d_1}\right) = 0, \quad \text{for} \quad j < 0$$

$$\frac{du_0}{dt} + c\left[\alpha\left(\frac{u_0 - u_{-1}}{d_1}\right) + \beta\left(\frac{u_1 - u_0}{d_2}\right)\right] = 0, \quad \alpha + \beta = 1$$

$$\frac{du_j}{dt} + c\left(\frac{u_{j+1} - u_{j-1}}{2d_2}\right) = 0, \quad \text{for} \quad j > 0 \tag{8.45}$$

Let $J = 0$ without loss of generality. Define

$$p_1 = k_0 d_1\,,\ p_2 = k d_2\,, \tag{8.46}$$

where k_0 is the incident wave number, and k is the wave number for $j \geq 0$. The solution for $j \leq 0$ is given by:

$$u_j = e^{i(jp_1 - \omega t)} + r(-1)^j e^{-i(jp_1 + \omega t)} \quad , \tag{8.47}$$

where

$$\omega = c\frac{\sin p_1}{d_1} . \tag{8.48}$$

The solution for $j \geq 0$ is

$$u_j = Re^{i(jp_2 - \omega t)} \quad , \tag{8.49}$$

where

$$\omega = \frac{c \sin p_2}{d_2} . \tag{8.50}$$

The frequency, ω, must be the same in both parts of the domain. Equating (8.48) and (8.50) gives

$$\sin p_2 = \frac{d_2}{d_1} \sin p_1 . \tag{8.51}$$

This relates p_2 to p_1, or k to k_0.

Since the incident wave must have $c_g^* > 0$ (this is what is meant by "incident"), we know that

$$0 < k_0 d_1 < \frac{\pi}{2}. \tag{8.52}$$

It follows that the wavelength of the incident wave is longer than $4d_1$.

Now consider several cases:

1. $d_2/d_1 > 1$. This means that the wave travels from a relatively fine grid to a relatively coarse grid. Let

$$\sin p_2 = \frac{d_2}{d_1}\sin p_1 \equiv a \ . \tag{8.53}$$

This implies that

$$e^{ip_2} = \pm\sqrt{1-a_2} + ia \ . \tag{8.54}$$

Since we can choose d_1, d_2, and k_0 any way we want, it is possible to make $\sin p_2 > 1$ or ≤ 1. We consider these two possibilities separately.

a) $a \equiv \sin p_2 > 1$. In this case, p_2 has to be complex. From (8.54),

$$e^{ip_2} = i(a \pm \sqrt{a^2-1}) = e^{i\frac{\pi}{2}}(a \pm \sqrt{a^2-1}) \ . \tag{8.55}$$

Here we have used $i = e^{i\,\pi/2}$. The solution for $j \geq 0$ is then

$$u_j = R(a \pm \sqrt{a^2-1})^j e^{i\left(\frac{\pi}{2}j - \omega t\right)} \ . \tag{8.56}$$

Since $a > 1$ by assumption, it is clear that $a + \sqrt{a^2-1} > 1$ and $a - \sqrt{a^2-1} < 1$. To ensure that u_j remains bounded as $j \to \infty$, we must choose the minus sign. Then

$$u_j = R(a - \sqrt{a^2-1})^j e^{i\left(\frac{\pi}{2}j - \omega t\right)} \tag{8.57}$$

The wavelength is $4d_2$, and the amplitude decays as j increases, as shown in the sketch.

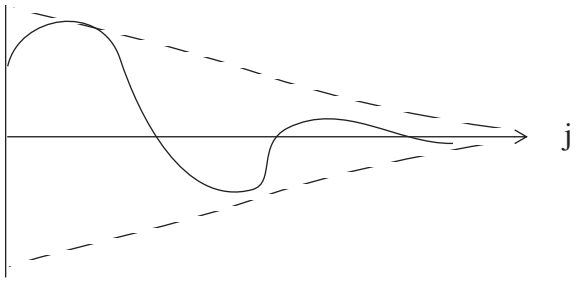

b) $a \equiv \sin p_2 \leq 1$. In this case p_2 is real. Since $\sin p_2 \equiv a < 1$, we see that

$$|p_2| < \frac{\pi}{2}. \tag{8.58}$$

This implies that $L = \frac{2\pi}{k} > 4d_2$. The solution is

$$u_j = Re^{i(j\sin^{-1}a - \omega t)} \quad . \tag{8.59}$$

From (8.51), since we are presently considering $d_2/d_1 > 1$, we see that $p_2 > p_1$. We also have from (8.51) that

$$\frac{k}{k_0} = \frac{\left(\frac{\sin p_1}{p_1}\right)}{\left(\frac{\sin p_2}{p_2}\right)} . \tag{8.60}$$

We know that $\sin x/x$ is a decreasing function of x for $0 < x < \pi/2$. We conclude, then, that $k/k_0 > 1$. This means that the wavelength of the transmitted wave is less than that of the incident wave.

2. $d_2/d_1 < 1$. This means that the wave travels from a relatively coarse grid to a relatively fine grid. In this case, p_2 is always real. The analysis is similar to (I, b) above. It turns out that the wavelength of the transmitted wave is longer than that of the incident wave. Since $p_2 \leq \sin^{-1}(d_2/d_1)$, we can show that the maximum wavelength of the transmitted wave is

$$L_{max} = \frac{2\pi d_2}{\sin^{-1}(d_2/d_1)} . \tag{8.61}$$

When $d_2/d_1 = 1/2$, the maximum wavelength is $12d_2$.

Next, we find R and r. At $j = 0$, (8.47) and (8.49) must agree. Then

$$1 + r = R . \tag{8.62}$$

We are also given that

$$\frac{\partial u_0}{\partial t} + c\left[\alpha\left(\frac{u_0 - u_1}{d_1}\right) + \beta\left(\frac{u_1 - u_0}{d_2}\right)\right] = 0 \ . \tag{8.63}$$

We can substitute (8.47) and (8.49) into (8.63):

$$-i\omega R + c\left\{\frac{\alpha}{d_1}[1 - e^{-ip_1} + r(1 + e^{ip_1})] + \frac{\beta}{d_2}R(e^{ip_2} - 1)\right\} = 0 \quad . \tag{8.64}$$

Use (8.62) to eliminate r in (8.64), and solve for R:

$$R = \frac{-c\frac{\alpha}{d_1}(1 - e^{-ip_1} - 1 - e^{-ip_1})}{-i\omega + c\left[\frac{\alpha}{d_1}(1 + e^{ip_1}) + \frac{\beta}{d_2}(e^{ip_2} - 1)\right]} \ . \tag{8.65}$$

Now use (8.48) to eliminate ω. Also use $\alpha + \beta = 1$. The result is

$$R = \frac{2\cos p_1}{1 + \cos p_1 - \gamma(1 - \cos p_2)} \ , \tag{8.66}$$

where we have defined

$$\gamma \equiv \left(\frac{\beta}{\alpha}\right)\left(\frac{d_1}{d_2}\right) \ . \tag{8.67}$$

Substituting (8.66) back into (8.62) gives the reflection coefficient as

$$r = -\left[\frac{1 - \cos p_1 - \gamma(1 - \cos p_2)}{1 + \cos p_1 - \gamma(1 - \cos p_2)}\right] \ . \tag{8.68}$$

This is the basic result sought.

As a check, suppose that $d_1 = d_2$ and $\alpha = \beta = \frac{1}{2}$. Then $j = 0$ is "just another point," and so there should not be any computational reflection, and the transmitted wave should be identical to the incident wave. From (8.51), we see that for this case $k = k_0$ and $p_1 = p_2$. Then (8.66) and (8.68) give $R = 1$, $r = 0$, i.e. complete transmission and no reflection, as expected.

For $\alpha \to 0$ with finite d_1/d_2, we get $\gamma \to \infty$, $R \to 0$, and $|r| \to 1$, unless $\cos p_2 = 1$, which is the case of an infinitely long wave, i.e. $p_2 = 0$. This is like Nitta's "Method 1."

For $\beta \to 0$ with finite d_1/d_2, $\gamma \to 0$ so that

$$\begin{aligned} R &\to \frac{2\cos p_1}{1+\cos p_1} = 1 - \tan^2\left(\frac{p_1}{2}\right), \\ r &\to -\left(\frac{1-\cos p_1}{1+\cos p_1}\right) = -\tan^2\left(\frac{p_1}{2}\right). \end{aligned} \tag{8.69}$$

This is the result obtained with Nitta's "Method 5."

As $p_1, p_2 \to 0$, $R \to 1$ and $r \to 0$, regardless of the value of γ. When p_1 and p_2 are small but not zero,

$$\cos p_1 \cong 1 - \frac{p_1^2}{2}, \tag{8.70}$$

$$\cos p_2 \cong 1 - \frac{p_2^2}{2}, \tag{8.71}$$

and

$$p_2 \cong \left(\frac{d_2}{d_1}\right) p_1 . \tag{8.72}$$

Then we find that

$$\begin{aligned} R \cong \frac{2\left(1-\frac{p_1^2}{2}\right)}{2-\frac{p_1^2}{2}-\gamma\frac{p_2^2}{2}} &\cong \left(1-\frac{p_1^2}{2}\right)\left(1+\frac{p_1^2}{4}+\gamma\frac{p_2^2}{4}\right) \\ &\cong 1-\frac{p_1^2}{4}+\gamma\frac{p_2^2}{4} \\ &\cong 1-\frac{p_1^2}{4}\left[1-\gamma\left(\frac{d_2}{d_1}\right)^2\right] \end{aligned} \tag{8.73}$$

Choosing

$$\gamma = (d_1/d_2)^2 \tag{8.74}$$

gives $R = 1 + O(p_2^4)$. Referring back to (8.67), we see that this choice of γ corresponds to

$$\frac{\beta}{\alpha} = \frac{d_1}{d_2}. \tag{8.75}$$

This is a good choice of β/α, because it gives R close to one and $|r|$ close to zero. We can re-write (8.75) as

$$-\alpha d_1 + \beta/d_2 = 0. \tag{8.76}$$

It can be shown that (8.76) is the requirement for second-order accuracy at the "seam" between the two grids. Since the given equations have second-order accuracy elsewhere, (8.75) [and (8.76)] essentially express the requirement that the order of accuracy be spatially homogeneous.

8.5 Analysis of boundary conditions for the advection equation using the energy method

Consider the one-dimensional advection equation:

$$\frac{\partial u}{\partial t} + c\frac{\partial u}{\partial x} = 0 . \tag{8.77}$$

Multiplying (8.77) by $2u$, we obtain

$$\frac{\partial}{\partial t}u^2 + \frac{\partial}{\partial x}cu^2 = 0 . \tag{8.78}$$

This shows that u^2 is also advected by the current. Defining u^2 as the "energy", we see that cu^2 is the energy flux and $\frac{\partial}{\partial x}cu^2$ is the energy flux divergence.

Suppose that (8.77) is approximated by the differential difference equation:

$$\frac{\partial u_j}{\partial t} + c\frac{u_{j+1} - u_{j-1}}{2\Delta x} = 0 . \tag{8.79}$$

Multiplying (8.79) by $2u_j$, we obtain

$$\frac{\partial}{\partial t}u_j^2 + \frac{cu_j u_{j+1} - cu_{j-1}u_j}{\Delta x} = 0 , \tag{8.80}$$

Comparing (8.80) with (8.78), we see that $cu_j u_{j+1}$ and $cu_{j-1}u_j$ are the energy fluxes from grid point j to grid point $j+1$ 1, and from grid point $j-1$ to grid point j, respectively. Applying (8.80) to the grid point $j+1$ gives

$$\frac{\partial}{\partial t}u_{j+1}^2 + \frac{cu_{j+1}u_{j+2} - cu_j u_{j+1}}{\Delta x} = 0 . \tag{8.81}$$

By comparing (8.80) and (8.81), we see that $cu_j u_{j+1}$ represents the energy transferred from the grid point *j* to grid point *j*+1. This is illustrated in Fig. 8.7

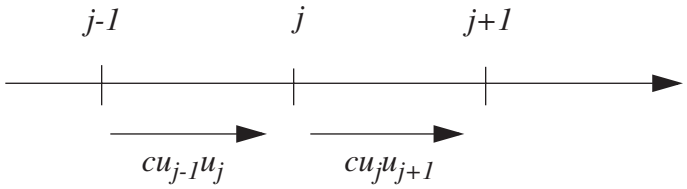

Figure 8.7: Sketch illustrating the energy fluxes that appear in (8.80).

In the differential case, the sign of the energy flux is the same as the sign of *c*. This is not necessarily true for the differential-difference equation, however, because $u_j u_{j+1}$ is not necessarily positive. When $u_j u_{j+1}$ is negative, as when *u* oscillates from one grid point to the next, the direction of energy flow is opposite to the direction of *c*. This implies negative c_g^* for $\frac{\pi}{2} < k\Delta x < \pi$. The implication is that for short waves, for which $u_j u_{j-1} < 0$, energy flows in the $-x$ direction, i.e. "backward." This is consistent with our earlier analysis of the group speed.

When we put an *artificial* boundary at $j = J$, and if we let $u_J = 0$ as in Nitta's Method 1, the energy flux from the point $J-1$ to the point *J* is zero. This is possible only when a computational mode, which transfers energy in the upstream direction, is superposed. This is a tip-off that Nitta's Method 1 is bad.

For Nitta's Method 2, $u_J = u_{J-1}$. This gives

$$cu_J u_{J-1} = cu_J^2 > 0 . \tag{8.82}$$

Since energy can leave the domain, there is less reflection. Of course, using the present approach, the actual energy flux cannot be determined, because we do not know the value of

u_J.

For Nitta's Method 4, $u_J = u_{J-2}$. Then for short waves

$$cu_{J-1}u_J = cu_{J-1}u_{J-2} < 0 . \tag{8.83}$$

This is bad.

For Nitta's Method 5,

$$u_J = 2u_{J-1} - u_{J-2} , \tag{8.84}$$

so

$$cu_Ju_{J-1} = cu_{J-1}(2u_{J-1} - u_{J-2}) = c(2u_{J-1}^2 - u_{J-1}u_{J-2}) . \tag{8.85}$$

For very short waves,

$$u_{J-1}u_{J-2} < 0 , \tag{8.86}$$

so that the flux given by (8.85) is positive, as it should be.For very long waves,

$$u_{J-1}u_{J-2} \cong u_{J-1}u_{J-1} , \tag{8.87}$$

so the flux is approximately

$$cu_Ju_{J-1} \cong cu_{J-1}^2 > 0 . \tag{8.88}$$

For Nitta's Method 7,

$$\frac{\partial u_J}{\partial t} + c\frac{u_J - u_{J-1}}{\Delta x} = 0 , \tag{8.89}$$

so we find that

$$\frac{\partial u_J^2}{\partial t} + 2c\frac{u_J^2 - u_Ju_{J-1}}{\Delta x} = 0 . \tag{8.90}$$

The energy flux "into J" is u_Ju_{J-1}, while that "out of J" is $u_J^2 > 0$. Applying (8.80) at J,

$$\frac{\partial}{\partial t}(u_{J-1}^2) + c\frac{u_{J-1}u_J - u_{J-2}u_{J-1}}{\Delta x} = 0 . \tag{8.91}$$

This shows that the energy flux out of $J-1$ is the same as the flux into J, which is good.

8.6 Physical and computational reflection of gravity waves at a wall

Now we discuss

$$\frac{\partial u_j}{\partial t} + g\frac{h_{j+1} - h_{j-1}}{2\Delta x} = 0 , \tag{8.92}$$

$$\frac{\partial h_j}{\partial t} + H\frac{u_{j+1} - u_{j-1}}{2\Delta x} = 0 , \tag{8.93}$$

which are, of course, differential-difference analogs of the one-dimensional shallow water equations. Consider a distribution of the dependent variables on the grid as shown in Fig. 8.8.

The wave solutions of (8.92) and (8.93) are

$$(u_j, h_j) \propto e^{i(kj\Delta x - \omega t)} , \tag{8.94}$$

giving

$$\omega u_j - g h_j \frac{\sin(k\Delta x)}{\Delta x} = 0 ,$$

$$\omega h_j - H u_j \frac{\sin(k\Delta x)}{\Delta x} = 0 . \tag{8.95}$$

Since u_j and h_j are not both identically zero, we obtain the familiar dispersion relation

$$\omega^2 = k^2 g H\left(\frac{\sin p}{p}\right)^2 \text{ where } p \equiv k\Delta x . \tag{8.96}$$

As discussed in Chapter 5, there are four solutions for a given value of ω, i.e. $p = p_0$, $p = -p_0$, $p = \pi - p_0$ and $p = -(\pi - p_0)$. In general, for a given ω, the solution for u_j is a linear combination of the four modes, and can be written as

$$u_j = [Ae^{ip_0 j} + Be^{-ip_0 j} + Ce^{i(\pi - p_0)j} + De^{-i(\pi - p_0)j}]e^{-i\omega t} . \tag{8.97}$$

By substituting (8.97) into (8.93), we find that h_j satisfies

$$h_j = \frac{H \sin p_0}{\omega \Delta x}[Ae^{ip_0 j} - Be^{-ip_0 j} + Ce^{i(\pi - p_0)j} - De^{-i(\pi - p_0)j}]e^{-i\omega t} . \tag{8.98}$$

If we assume ω>0, so that $\sin p_0 = \frac{\omega \Delta x}{\sqrt{gH}}$ [see (8.96)], then (8.98) reduces to

$$h_j = \sqrt{\frac{H}{g}}\left[ae^{ip_0 j} - be^{-ip_0 j} + ce^{i(\pi - p_0)j} - de^{i(\pi - p_0)j}\right]e^{-i\omega t} . \tag{8.99}$$

Consider an incident wave traveling toward the right with a certain wave number k_0, such that $0 < p_0 (\equiv k_0 \Delta x) < \pi$. Since we are assuming $\omega > 0$, $e^{ip_0 j}\ e^{-i\omega t}$ represents such a wave.

Two additional waves can be produced by reflection at the boundary. We assume that the amplitude of the incident wave with $p = p_0$ is 1, and that of the reflected wave with $p = -p_0$ is R, and that of the reflected wave with $p = \pi - p_0$ is r. In other words, we take $A = 1, B = R, C = r$, and $D = 0$. Then (8.97) and (8.99) can be written as

$$u_j = \left[e^{ip_0 j} + Re^{-ip_0 j} + re^{i(\pi - p_0)j}\right]e^{-i\omega t} , \tag{8.100}$$

$$h_j = \sqrt{\frac{H}{g}}\left[e^{ip_0 j} - Re^{-ip_0 j} + re^{i(\pi - p_0)j}\right]e^{-i\omega t} . \tag{8.101}$$

Now suppose that at $j = J$ we have a rigid wall (a real, physical wall). Since there is no flow through the wall, we know that $u_J = 0$, for all time. This is a physical boundary condition. Also, $\left(\frac{\partial h}{\partial x}\right)_J = 0$ is required, because otherwise there would be a pressure gradient which would cause u_J to change with time. Consider two possible methods for approximating this:

$$\text{Method I: } u_J = 0, \quad h_J - h_{J-1} = 0 , \tag{8.102}$$

$$\text{Method II: } u_J + u_{J-1} = 0, \quad h_J - h_{J-1} = 0 . \tag{8.103}$$

Method II essentially corresponds to placing the wall at $J - 1/2$ rather than at J. Then u is assumed to be antisymmetric and h is assumed to be symmetric about the wall.

A third method is to predict h_j using uncentered differencing:

$$\text{Method III: } u_J = 0, \quad \frac{\partial h_J}{\partial t} + H\left(\frac{0 - u_{J-1}}{\Delta x}\right) = 0 . \tag{8.104}$$

This is equivalent to assuming $u_{J+1} = -u_{J-1}$, and then applying (8.93) to the point J.

In a straightforward manner, the R's and the r's can be determined for each of Methods I, II, and III. Table 5.1 gives the expressions for R and r for each method, and Fig. 8.8 shows

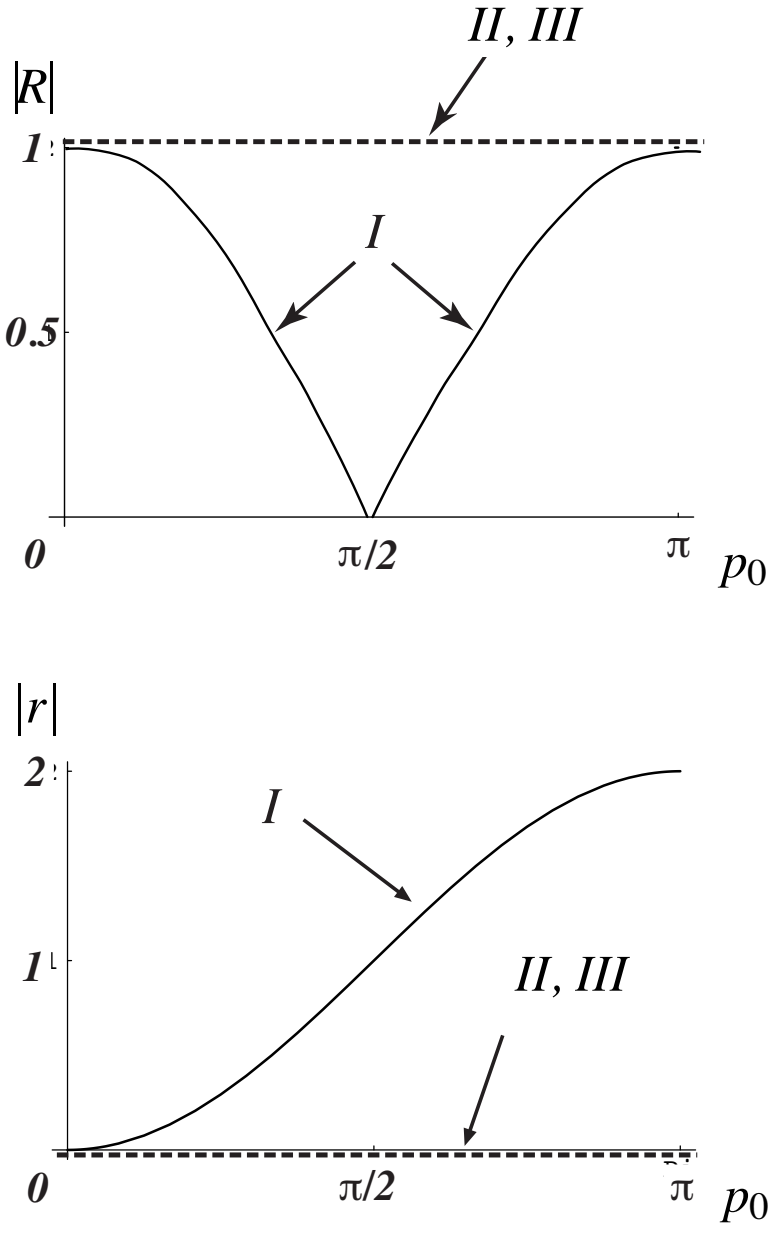

Figure 8.8: The upper panel shows the variation of $|R|$ with p_0 for Methods I, II, and III. The lower panel shows the corresponding results for $|r|$.

$|R|$ and $|r|$ plotted as functions of p_0. Method I is obviously bad. False energy is produced

Table 8.2: Expressions for R and r, for Methods I, II, and III.

	Method I	Method II	Method III
R	$-\cos\ p_0$	$-\cos\ p_0 + i \sin\ p_0$ $(\|R\| = 1)$	-1
r	$-1 + \cos\ p_0$	0	0

when p_0 is close to π. Even when p_0 is small, part of the incident energy is reflected back with $p = \pi - p_0$, and the solution will become "noisy". Methods II and III are better. Method III is best.

A way to bypass most of the problems associated with the existence of too many modes is to use a grid with a "staggered" spatial distribution of the dependent variables, as shown in Fig. 8.9. Note that u is defined "at the wall," where $j = J$. If we are dealing with a rigid wall, the boundary condition $u_J = 0$ is sufficient because h is not defined at the boundary. Use of this staggered grid means use of either only circled or only boxed quantities in Fig. 8.8.

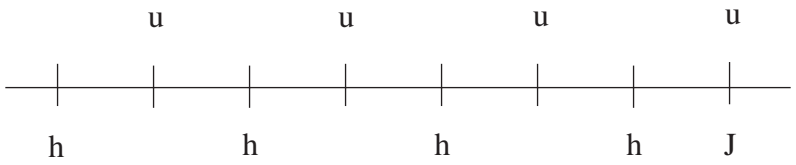

Figure 8.9: A one-dimensional staggered grid for solution of the shallow water equations, near a wall where $j = J$.

8.7 Boundary conditions for the gravity wave equations with an advection term

We now generalize our system of equations to include advection by a mean flow U, in the following manner:

$$\left(\frac{\partial}{\partial t} + U\frac{\partial}{\partial x}\right)u + g\frac{\partial h}{\partial x} = 0\ , \tag{8.105}$$

$$\left(\frac{\partial}{\partial t} + U\frac{\partial}{\partial x}\right)v = 0 , \tag{8.106}$$

$$\left(\frac{\partial}{\partial t} + U\frac{\partial}{\partial x}\right)h + H\frac{\partial u}{\partial x} = 0 . \tag{8.107}$$

We have also added a velocity component, v, in the y-direction. The system is still linear, but it is getting more realistic! The dependent perturbation quantities u, v, and h are assumed to be constant in y. In this sense the problem is one-dimensional, even though $v \neq 0$ is allowed.

Since (8.105) through (8.107) are hyperbolic, we can write them in normal form:

$$\left[\frac{\partial}{\partial t} + (U+c)\frac{\partial}{\partial x}\right]\left(u + \sqrt{\frac{g}{H}}h\right) = 0 , \tag{8.108}$$

$$\left(\frac{\partial}{\partial t} + U\frac{\partial}{\partial x}\right)v = 0 , \tag{8.109}$$

$$\left[\frac{\partial}{\partial t} + (U-c)\frac{\partial}{\partial x}\right]\left(u - \sqrt{\frac{g}{H}}h\right) = 0 . \tag{8.110}$$

Here $c \equiv \sqrt{gH}$. We assume $c > |U|$, which is often true in the atmosphere. For (8.108) and (8.109), the lines $x-(U+c)t =$ constant and $x-(U-c)t =$ constant are the characteristics, and are shown as the solid lines in Fig. 8.10. Everything is similar to the case without advection, except that now the slopes of the two characteristics which involve c differ not only in sign but also in magnitude.

We also have an additional equation, namely (8.109). This, of course, is an advection equation, and so v is a constant along the lines $x - Ut =$ constant, which are shown schematically by the broken lines in Fig. 8.10. We should then specify v only on the inflow boundary. The divergence is given by $\frac{\partial u}{\partial x}$, and the vorticity by $\frac{\partial v}{\partial x}$. We conclude that for this one-dimensional case the normal or divergent component of the wind (u) can be specified at both boundaries, but the tangential or rotational component (v) can be specified only at the inflow boundary.

8.8 The energy method as a guide in choosing boundary conditions for gravity waves

From the gravity wave equations we can derive the total energy equation

$$\frac{\partial}{\partial t}\left(\frac{1}{2}Hu^2 + \frac{1}{2}gh^2\right) + gH\frac{\partial}{\partial x}(hu) = 0 . \tag{8.111}$$

Suppose that the gravity-wave equations are approximated by

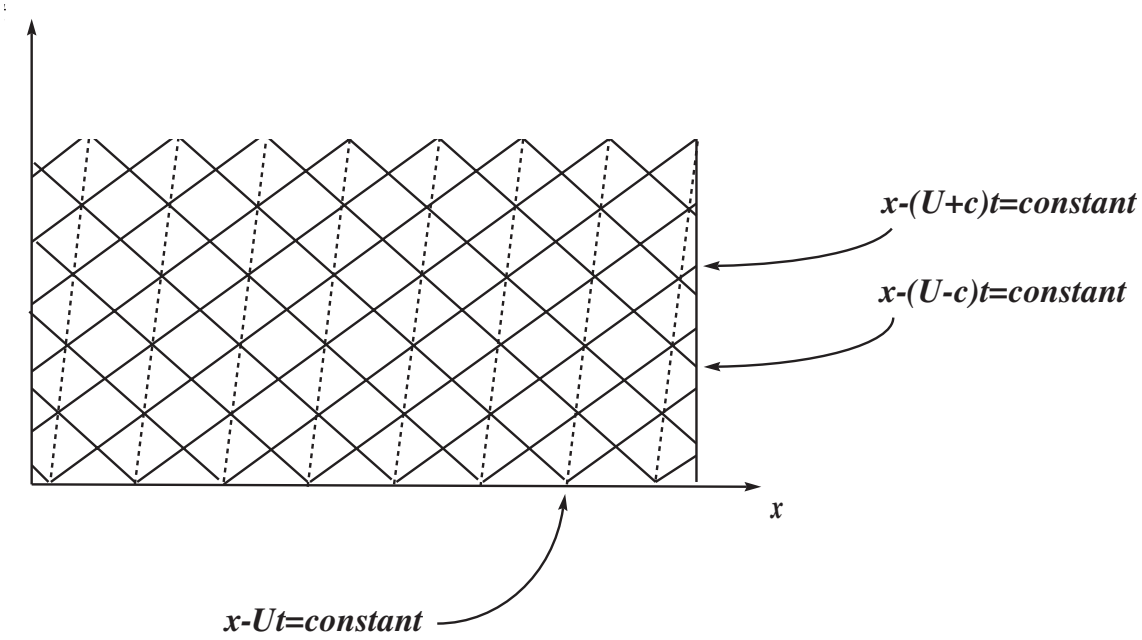

Figure 8.10: Characteristics for the case of shallow water wave propagation with an advecting current *U*.

$$\frac{\partial u_j}{\partial t} + g\frac{h_{j+1} - h_{j-1}}{2\Delta x} = 0 , \tag{8.112}$$

$$\frac{\partial h_j}{\partial t} + H\frac{u_{j+1} - u_{j-1}}{2\Delta x} = 0 . \tag{8.113}$$

The corresponding discretized total energy equation is

$$\frac{\partial}{\partial t}\left(\frac{1}{2}Hu_j^2 + \frac{1}{2}gh_j^2\right) + gH\left[\frac{\frac{1}{2}(u_j h_{j+1} + u_{j+1}h_j) - \frac{1}{2}(u_{j-1}h_j + u_j h_{j-1})}{\Delta x}\right] = 0 . \tag{8.114}$$

Earlier, $u = \sqrt{\frac{g}{H}}h$ was recommended as a computational boundary condition at the artificial boundary BB'. Correspondingly, if we let

$$h_J = \sqrt{\frac{H}{g}}u_{J-1}, \quad u_J = \sqrt{\frac{g}{H}}h_{J-1} , \tag{8.115}$$

then the energy flux from the point $J-1$ to the point J becomes

$$gH\frac{1}{2}(u_{J-1}h_J + u_J h_{J-1}) = \sqrt{gH}\left(\frac{1}{2}Hu_{J-1}^2 + \frac{1}{2}gh_{J-1}^2\right) > 0 \tag{8.116}$$

which is guaranteed to be positive (outward energy flow).

When the boundary is a real, rigid wall, we may put it between the points $J-1$ and J, and let $u_J + u_{J-1} = 0$ and $h_J - h_{J-1} = 0$ (Method II). Then the energy flux is $gH\frac{1}{2}(u_{J-1}h_J + u_J h_{J-1}) = 0$. Alternatively, we may put the wall at the point J $(u_J = 0)$ and let

$$\frac{\partial h_J}{\partial t} + H\left(\frac{0 - u_{J-1}}{\Delta x}\right) = 0 \text{ (Method III)} . \tag{8.117}$$

The total energy equation at the point J is then

$$\frac{\partial}{\partial t}\frac{1}{2}gh_J^2 + gH\left(\frac{0 - h_J u_{J-1}}{\Delta x}\right) = 0 . \tag{8.118}$$

There is no kinetic energy term since $u_J = 0$. In (8.118), $gHh_J u_{J-1}$ is the energy flux from the point $J-1$ to the point J. Note, however, that $u_J h_{J-1} = 0$. There is no energy flux beyond the point J.

For the total energy equation (8.111), the boundary condition $u - \sqrt{\frac{g}{H}}h = 0$ gives

$$uh = \sqrt{\frac{g}{H}}h^2 > 0 , \tag{8.119}$$

so that there will be *outward* energy flux at the right boundary. From (8.114), we see that with a rigid wall, the energy flux at $J - \frac{1}{2}$ is $u_{J-1}h_J + u_J h_{J-1}$. We have already discussed three methods for giving boundary conditions on the wave equations.

For Method I, we find that

$$u_J = 0, \quad h_J - h_{J-1} = 0 , \tag{8.120}$$

the energy flux is

$$u_{J-1}h_{J-1} \tag{8.121}$$

which is generally different from zero. This means that total reflection does not occur.

Method II is

$$u_J + u_{J-1} = 0, \qquad h_J - h_{J-1} = 0 . \tag{8.122}$$

The energy flux is then

$$u_{J-1}h_J + u_J h_{J-1} = u_{J-1}h_{J-1} + (-u_{J-1})h_{J-1} = 0 , \tag{8.123}$$

so we have *complete reflection*.

8.9 Summary

Computational modes in space can be generated at real and / or artificial walls, and arise from space differencing schemes. In problems with boundaries, these modes can necessitate the introduction of "computational boundary conditions" at outflow boundaries. The computational modes have short wavelengths and move "backwards." Various methods can be used to minimize problems at boundaries, as discussed in the paper by Matsuno. None of these methods completely eliminates the problems caused by artificial boundaries, however.

Problem

1. Derive the form of $|r|$ for Nitta's Method 7. Assume that J is even.